Sonodynamic Treatment Triggers Cancer Cell Killing by Doxorubicin in P-Glycoprotein-Mediated Multidrug Resistant Cancer Models

ADVANCED THERAPEUTICS
www.advtherap.com

Sonodynamic Treatment Triggers Cancer Cell Killing by Doxorubicin in P-Glycoprotein-Mediated Multidrug Resistant Cancer Models

Federica Foglietta, Marta Giacone, Gianni Durando, Roberto Canaparo, and Loredana Serpe*

Doxorubicin is a widely used chemotherapeutic agent that can be hampered in its efficacy by the occurrence of multidrug resistance (MDR), due to the overexpression of the drug efflux transporter P-glycoprotein. As overcoming MDR still remains an unmet clinical need, this work aims at investigating an innovative strategy. Sonodynamic therapy (SDT) selectively kills cancer cells by combining low-intensity ultrasound (US) with a responsive chemical agent (sonosensitiser) that can be activated to produce reactive oxygen species (ROS). Therefore, the efficacy of SDT, using doxorubicin as sonosensitiser, is studied on human MDR ovarian (A2780/MDR) and colon (HT-29/MDR) cancer cells. The ultrasound exposure of MDR cells pre-incubated with non-cytotoxic concentrations of doxorubicin for 1 h has induced a statistically significant decrease of cell proliferation after 72 h. Interestingly, US has selectively triggered the ROS-mediated cytotoxicity of the doxorubicin entrapped into the cancer cell membrane leading to necrotic cancer cell death by lipid peroxidation. Moving from 2D to 3D HT-29/MDR cell cultures, the ability of SDT to reduce the growth of MDR spheroids by inducing significant necrotic cancer cell death is also confirmed. In conclusion, SDT can have a role in treating MDR tumors by eliciting the ROS-mediated cytotoxicity of doxorubicin.

1. Introduction

The multifaceted phenomenon of drug resistance still remains the most relevant factor limiting cancer cure.[1] In particular, multidrug resistance (MDR) refers to the intrinsic or acquired ability of cancer cells to become resistant to various structurally untreated drugs acting by different mechanisms.[2] According to the current understanding, MDR is characterized by a reduced drug accumulation due to the overexpression of ATP-binding cassettes (ABC) transporters such as P-glycoprotein (P-gp).[3,4]

P-gp is a 170 kDa membrane protein that exhibits energy-dependent transport of cationic lipophilic compounds but also classic anticancer chemotherapeutic drugs, such as vinblastine, doxorubicin, and paclitaxel, and many of the "new generation" of cancer targeted small molecules (e.g., kinase inhibitors).[5] That is why P-gp has been widely targeted in drug resistance reversal studies. The general strategy to overcome the P-gp-mediated MDR consists in the coadministration of anticancer drugs with i) chemical inhibitors of P-gp leading to increased drug accumulation into cancer cells and cancer cell killing or ii) P-gp substrates achieving a similar effect by competition for the transport process.[5] Unfortunately, the strategy of developing potent and selective P-gp inhibitors has encountered several drawbacks including disruption of key barrier tissues and severe toxicity. Moreover, the use of P-gp substrates seems to be not an adequate approach to counter drug resistance, therefore innovative strategies are needed. Recently, the administration of anticancer drugs via micro- and nano-particles or polymers and the modulation and/or inhibition of P-gp expression could provide new therapeutic strategies for the prevention of MDR.[6–10] However, these approaches have not yet reached clinical success due to the complex array of altered pharmacokinetics and drug toxicity.

In this scenario, recent evidence supports investigations of physical strategies, such as low-intensity ultrasound (US), to reverse P-gp-mediated MDR.[11] Indeed, according to the modulation of US parameters, it has been reported that short- and long-term effects could be achieved, such as intracellular drug accumulation due to the increased permeability of cancer cell membranes (i.e., sonoporation), and cancer cell death due to US-mediated cancer cell membrane disruption or intramembrane drug activation (i.e., sonodynamic therapy, SDT).[12]

F. Foglietta, M. Giacone, R. Canaparo, L. Serpe
Department of Drug Science and Technology
University of Torino
Torino 10125, Italy
E-mail: roberto.canaparo@unito.it
G. Durando
National Institute of Metrological Research (INRIM)
Strada delle Cacce 91, Torino 10135, Italy

The ORCID identification number(s) for the author(s) of this article can be found under https://doi.org/10.1002/adtp.202400070

DOI: 10.1002/adtp.202400070

In particular, SDT is a reactive oxygen species (ROS)-based therapy, as photodynamic therapy (PDT), that exploits US to trigger a responsive agent (i.e., sonosensitizer), in presence of oxygen, for achieving selective cancer cell killing with low side effects in healthy tissues. This anticancer strategy consists in a remotely controlled activation of a chemical agent by US possessing higher tissue penetration compared to light used in PDT.[13,14] This suggests that SDT could be applied more widely to tumor cases as a non-invasive treatment for solid tumors that were previously too deep-sited to be treated with PDT.[15] The mechanism through which SDT exerts its efficacy is still under debate, however sonoluminescence, a phenomenon in which the energy is generated by bubbles that collapse during US-induced acoustic cavitation, is considered as a responsible one.[16]

Among the sensitizer used in SDT, doxorubicin (Doxo), an anticancer drug that exerts its cytotoxicity by different mechanisms, involving topoisomerase IIα inhibition and ROS production, shows interesting sonodynamic properties.[17] Nevertheless, Doxo presents different problems that reduced its clinical applications, indeed cytotoxicity induced by Doxo is responsible of many side effects, some of them easy-manageable such as nausea and diarrhea, but also more impactful such as myelosuppression and cardiotoxicity.[18]

In a previous work, we investigated the efficacy of SDT with Doxo both in a human Doxo non-resistant ovarian cancer (OC) cell line (A2780/WT) and in a human Doxo-resistant OC cell line (A2780/MDR).[17] Doxo was used at very low concentrations, in order to avoid its significant side effects, but being still able to promote, as sonosensitiser, cancer cell death in A2780/WT cells. Since Doxo is a well know P-gp substrate it was also explored whether A2780/MDR cells could be affected by SDT. Interestingly, in A2780/MDR cells it was observed a significant cytotoxic effect but at a significantly different Doxo concentration and incubation time compared to the treatment of A2780/WT cells (0.5 μM for 1 h in A2780/MDR cells and 0.05 μM for 24 h in A2780/WT cells) suggesting the ability of US exposure to induce cancer cell killing also in MDR ovarian cancer cells exposed to Doxo.[17] The present work therefore aims to more broadly investigate this US-based approach to counteract P-gp-mediated MDR, also optimising the US parameters compared to our previous work[17] on the human Doxo-resistant ovarian carcinoma cell line, A2780/MDR, and colon carcinoma cell line, HT-29/MDR, grown as 2D and 3D cell cultures.

2. Results

2.1. Doxorubicin Cytotoxicity and Cellular Uptake in A2780 and HT-29 2D Cell Cultures

According to our previous work, the IC_{50} of Doxo at 24 h was 1.66 ± 0.19 μM in A2780/WT cells and above 100.00 μM in A2780/MDR cells, leading to the selection of Doxo 0.05 μM in A2780/WT cells and 0.5 μM in A2780/MDR cells as the proper non-cytotoxic concentration for the sonodynamic treatment (concentration lower than the respective IC_{05}).[17]

HT-29/WT and HT-29/MDR cell lines were incubated with increasing concentrations of Doxo to determine the IC_{50} at 24 h that was 2.72 ± 0.17 μM in HT-29/WT cells and above 100.00 μM in HT-29/MDR cells. Therefore, it was decided to perform the US-based treatment at the non-cytotoxic Doxo concentration of 0.5 μM in HT-29/WT cells and 1.0 μM in HT-29/MDR cells (concentration lower than the respective IC_{05}).

To verify the Doxo internalization after 1, 6, 12, and 24 h of incubation, A2780/WT and A2780/MDR cells were incubated with Doxo 0.05 and 0.5 μM, respectively, whereas HT-29/WT and HT-29/MDR cells were incubated with Doxo 0.5 and 1 μM, respectively. In A2780/WT cells, the largest increase in the cellular uptake of Doxo at 0.50 μM was detected after 24 h compared to 1 h of incubation (integrated mean fluorescence intensity, iMFI, at 24 h 716.92 ± 151.10 and at 1 h 107.33 ± 19.45, $p \leq 0.001$), whereas at 0.05 μM only a slight increase in the cellular uptake of Doxo was observed after 24 h compared to 1 h of incubation (**Figure 1**). Furthermore, observing the Doxo signal in A2780/MDR cells, very similar and low iMFI values were detected only with 0.50 μM Doxo at any time of incubation (Figure 1), corresponding to an important reduction of the drug's uptake in A2780/MDR cells compared to A2780/WT cells.

In HT-29/WT cells, at both the concentration tested (0.50 and 1.0 μM) the largest increase in the cellular uptake of Doxo was detected after 24 h compared to 1 h of incubation (for 0.5 μM Doxo iMFI at 24 h 20.47 ± 0.12 and at 1 h 5.32 ± 0.12, $p \leq 0.01$; for 1.0 μM Doxo iMFI at 24 h 281.65 ± 29.56 and at 1 h 107.62 ± 10.48, $p \leq 0.001$) (Figure 1). Furthermore, observing the Doxo signal in HT-29/MDR cells, very similar and low iMFI values were detected with 0.50 and 1.0 μM Doxo, at any time of incubation, as the statistical analysis did not show any statistically significant differences in the Doxo uptake (Figure 1), corresponding to an important reduction of the drug's uptake in HT-29/MDR cells compared to HT-29/WT cells.

These data are in line with the resistant phenotype of the MDR cell lines that was confirmed by a cytofluorimetric functional analysis of P-gp by using calcein-AM, a substrate of P-gp able to highlight differences in its internalization due to P-gp activity. The cytofluorimetric data of the MDR cell lines were compared with the ones obtained from the analysis of WT cell lines. **Figure 2A** shows the intracellular calcein-AM that was significantly lower in A2780/MDR cells ($2.57 \times 10^7 \pm 6.53 \times 10^6$) than in A2780/WT cells ($8.87 \times 10^8 \pm 4.55 \times 10^4$, $p \leq 0.001$) as in HT-29/MDR cells ($7.25 \times 10^8 \pm 1.99 \times 10^7$) than in HT-29/WT cells ($1.36 \times 10^9 \pm 9.63 \times 10^7$, $p \leq 0.01$). Furthermore, to confirm the resistant phenotype in A2780/MDR and HT-29/MDR cells, the P-gp level of expression was also evaluated by its cytofluorimetric detection and Figure 2B shows the cytofluorimetric analysis highlighting the higher level of P-gp expression detected in the MDR cell lines compared to the WT cell lines.

2.2. Doxorubicin Cellular Localization in A2780/MDR and HT-29/MDR 2D Cell Cultures

Although the cytofluorimetric analysis of Doxo uptake in the MDR cell lines showed very low levels of the drug after 1 h of incubation (Figure 1), it was decided to verify its intracellular distribution by fluorescence microscopy since we set up US exposure at that time of Doxo incubation. **Figure 3** shows that Doxo is not localized into the nuclei but around the cell membrane forming characteristic spots probably related to P-gp activity. Fur-

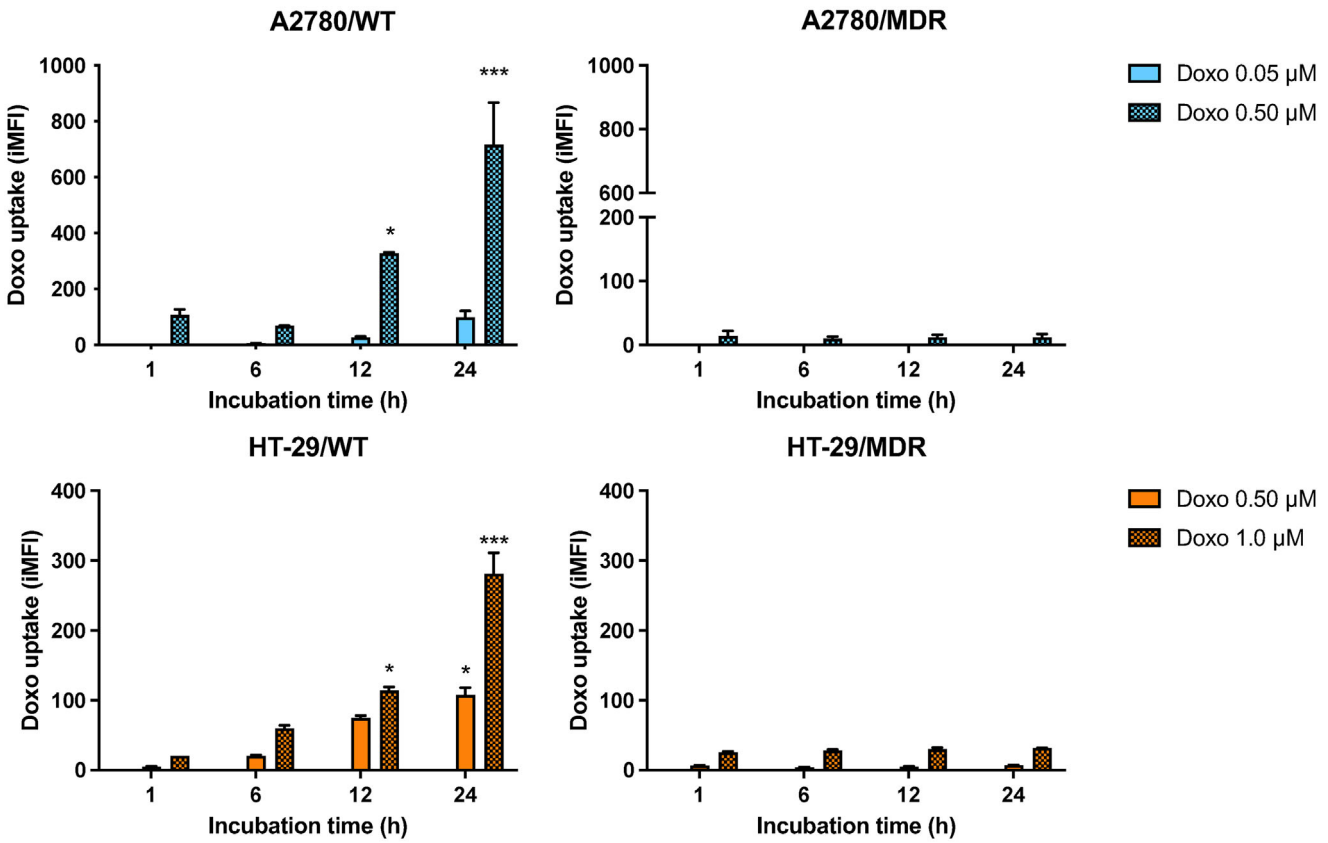

Figure 1. Doxo cellular uptake in WT and MDR cell lines. According to the cytotoxicity data A2780/WT and A2780/MDR cells were exposed to Doxo 0.05 and 0.50 μM for 1, 6, 12, and 24 h, whereas HT-29/WT and HT-29/MDR cells were exposed to Doxo 0.50 and 1.0 μM for 1, 6, 12, and 24 h. Data are expressed asiMFI. Statistical significance of Doxo uptake after 24 h versus 1 h of incubation: $^{*}p \leq 0.05$, $^{***}p \leq 0.001$.

thermore, by observing the Doxo localization in A2780/WT and in HT-29/WT cells, the spots are not visible and Doxo is mainly localized at nuclei level.

2.3. Effects of US Exposure on Cell Membrane Fluidity of A2780/MDR and HT-29/MDR 2D Cell Cultures

Considering the mechanical nature of the physical stimulus applied, i.e., US, the cell membrane fluidity of MDR cell lines before and after US exposure was investigated by the merocyanine 540 (MC540) assay. In particular, it was highlighted the pivotal role of the interaction between US and cell membrane in eliciting the US-mediated energy transfer in the form of intramembrane cavitation according to the bilayer sonophore (BLS) theory,[19] that can be responsible for the activation of the sonosensitizer.

Figure 4 shows the iMFI values for MC-540 distinguishing between untreated and US-treated MDR cell lines. In A2780/MDR cells, after US-exposure the cell membrane fluidity was modified as it was significantly decreased compared to untreated cells ($p \leq 0.05$). Nevertheless, a reduction in the membrane fluidity was also observed in HT-29/MDR cells after US exposure compared to untreated cells ($p \leq 0.05$). This analysis then revealed that, at the selected US parameters, the US exposure is able to influence the membrane fluidity, therefore suggesting a possible sonodynamic effect in the presence of an appropriate chemical agent as Doxo, according to BLS theory.[19]

2.4. Effect of Sonodynamic Treatment on A2780/MDR and HT-29/MDR 2D Cell Cultures

Based on the data obtained from the above-mentioned cytotoxicity and cellular uptake studies, the concentrations and incubation times for Doxo to act as a sonosensitizer were set at 0.50 μM for 1 h in A2780/MDR cells and at 1 μM for 1 h in HT29/MDR cells. Cells were then exposed to US and the treatment effect on cell proliferation was monitored at 24 and 72 h. In A2780/MDR cells, a statistically significant reduction in cell proliferation was observed after 72 h ($p \leq 0.01$), compared to untreated cells (Ctrl), while no significant decrease in cell proliferation was noticed when cells were exposed to Doxo and US separately. It is worth emphasizing that similar effects on cell proliferation were also noted after each set of treatment conditions in HT-29/MDR cells with a statistically significant reduction in cell proliferation only after the US-exposure of Doxo-pre-incubated cells at 72 h compared to untreated cells (Ctrl, $p \leq 0.05$) (**Figure 5**). Therefore, this evidence suggests a sonodynamic activation of the Doxo entrapped into the cell membrane or nearby the cell membrane of both the resistant ovarian and colon cancer cell lines.

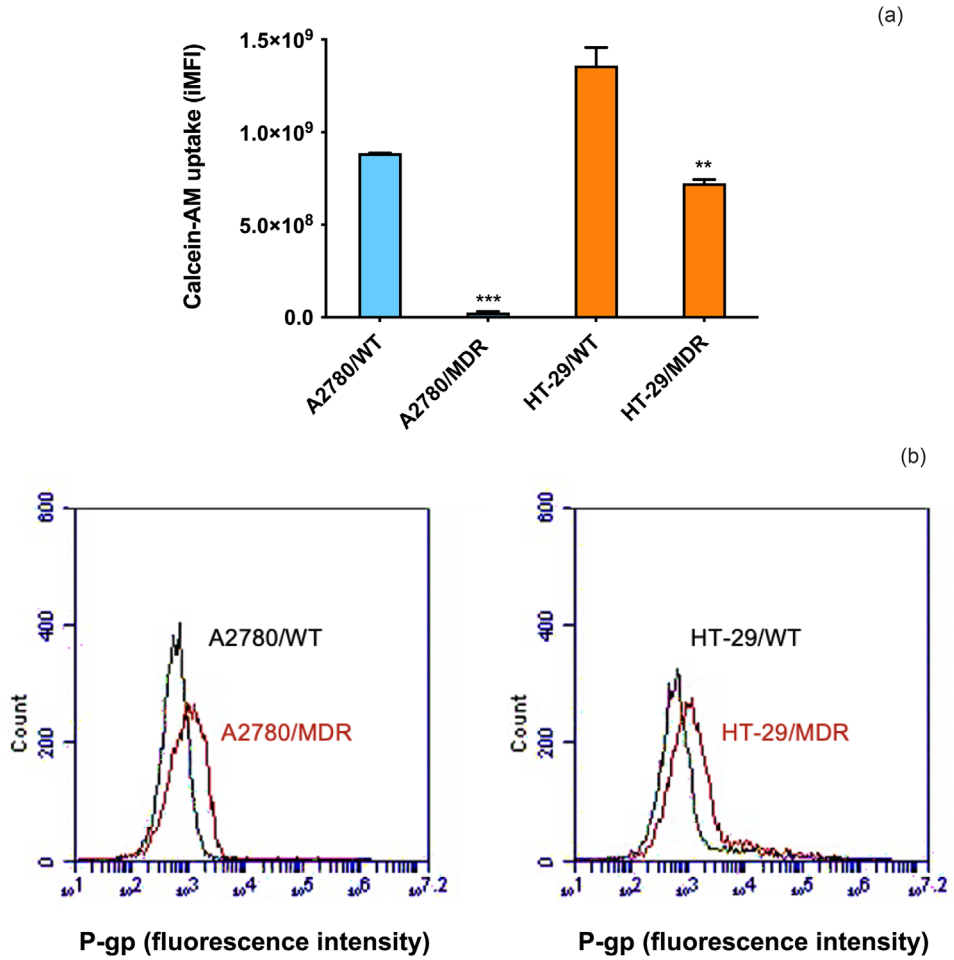

Figure 2. P-gp activity and expression in A2780 and HT-29 cell lines. a) The iMFI values of calcein-AM, a substrate of P-gp, highlight a significant difference of P-gp activity between WT and MDR cell lines by cytofluorimetric analysis. Statistical significance of P-gp activity of WT versus MDR cell lines: $^{**}p \leq 0.01$, $^{***}p \leq 0.01$. b) Flow cytometry plots of P-gp expression analyzed as fluorescence intensity in WT and MDR cell lines.

To confirm whether the previous results were only due to a sonodynamic activation and not to a sonoporation mechanism, a cytofluorimetric analysis of Doxo internalization was performed on both MDR cell lines before and just after US treatment. As shown in **Figure 6**, no increase in Doxo uptake was observed after US exposure compared to untreated cells, confirming that the cytotoxicity observed after US treatment (Figure 5) was not related to an increase in drug internalization through a sonoporation mechanism.

2.5. Cell Death Induced by Sonodynamic Treatment on A2780/MDR and HT-29/MDR 2D Cell Cultures

Cell death evaluation after SDT on resistant cell lines were carried out 48 h after SDT by cytofluorimetric analyses. When A2780/MDR cells underwent to SDT (Doxo + US treatment), as showed in **Figure 7**, after 48 h a statistical reduction of viable cells was observed (34.35% ± 2.11) compared to untreated cells (Ctrl, 71.65% ± 1.41, $p \leq 0.001$), along with a statistically significant increase in late apoptotic/necrotic cells (59.56% ± 3.50) compared to Ctrl (24.48% ± 0.47, $p \leq 0.001$); no significant increase in early apoptotic cells was observed compared to Ctrl. In HT-29/MDR cells, a significant decrease of viable cells (58.38% ± 0.65) was detected after SDT compared to Ctrl (81.07% ± 0.38, $p \leq 0.05$) along with a statistically significant increase in late apoptotic/necrotic cells (26.54% ± 3.94) and early apoptotic cells (14.09% ± 4.59) compared to the untreated cells (13.75% ± 1.146, $p \leq 0.05$, and 5.18% ± 1.527, $p \leq 0.05$, respectively). These data highlight that the US exposure of Doxo causes a significant cytotoxicity by mainly triggering necrotic cell death.

2.6. Lipid Peroxidation Induced by Sonodynamic Treatment on A2780/MDR and HT-29/MDR 2D Cell Cultures

Malondialdehyde (MDA) was evaluated as a marker of lipid peroxidation due to the cell damaging exerted by its electrophilic group.[20] A significant increase in lipid peroxidation was observed in A2780/MDR cells treated with Doxo and US compared to untreated cells ($p \leq 0.01$), as was also observed to an even greater extent in HT-29/MDR cells treated with Doxo and US

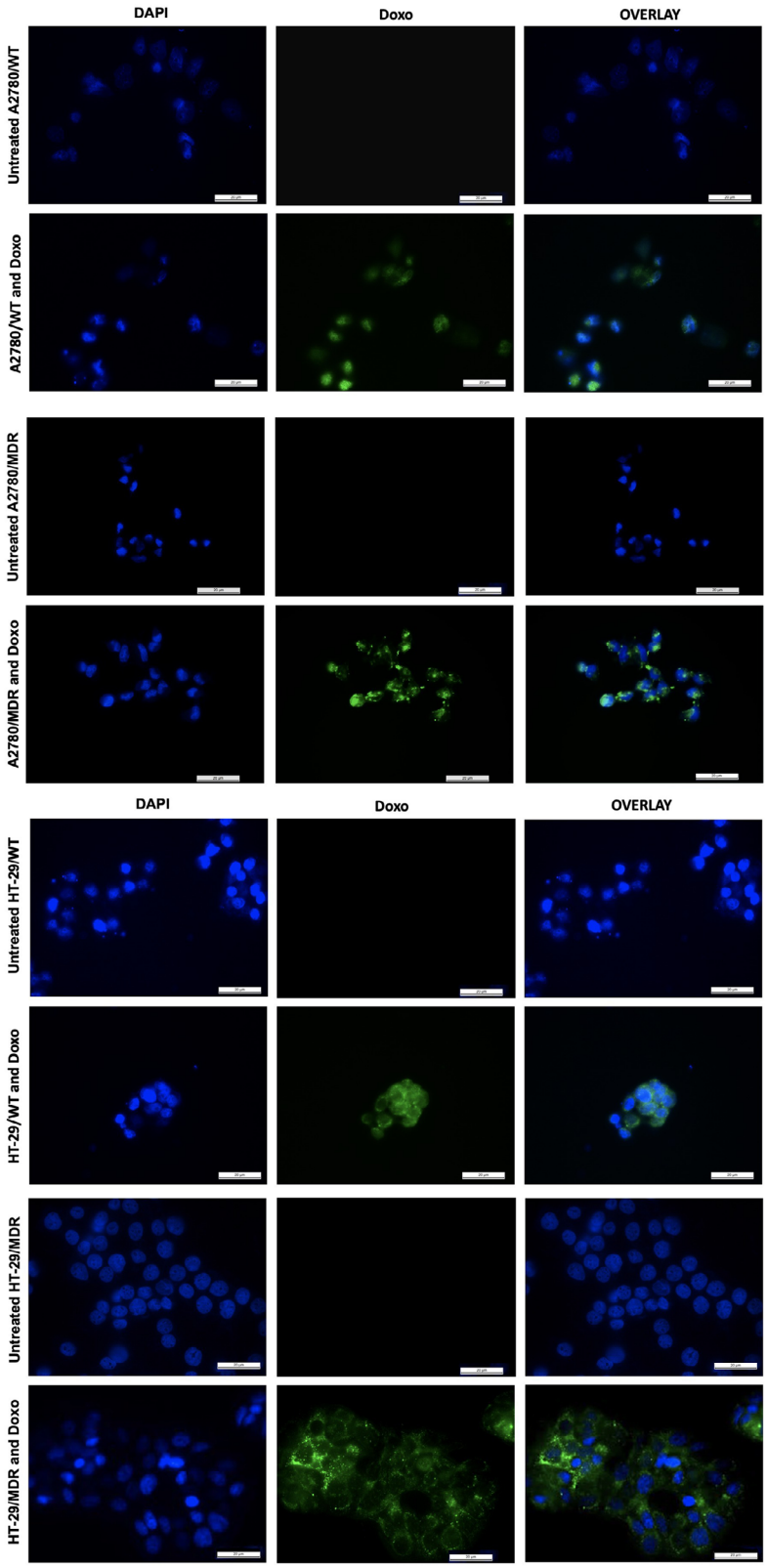

Figure 3. Representative images of Doxo localization in A2780/WT, A2780/MDR, HT-29/WT, and HT-29/MDR cell lines. Doxo was incubated for 1 h in A2780/WT and A2780/MDR cells at 0.5 μM and in HT-29/WT and HT-29/MDR cells at 1.0 μM. Fluorescent images of untreated and Doxo-treated cells show cell nuclei stained with 4', 6-diamidino-2-phenylindole (DAPI, blue), Doxo (green) and overlay images of cell nuclei and Doxo (magnification 40x and scale bar 20 μm).

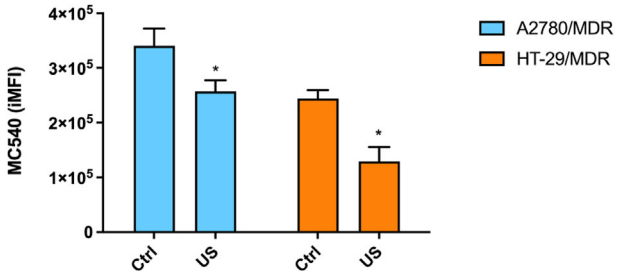

Figure 4. Effect of US exposure on cell membrane fluidity in A2780/MDR and HT-29/MDR cells. Cells were incubated with MC540 and treated with US (0.63 W cm^{-2}, 1.505 MHz, 3 min, 70% duty cycle, DC). Data are expressed as iMFI of MC540 positive cells. Statistical significance of untreated cells (Ctrl) versus US-treated cells: $^{*}p \leq 0.05$.

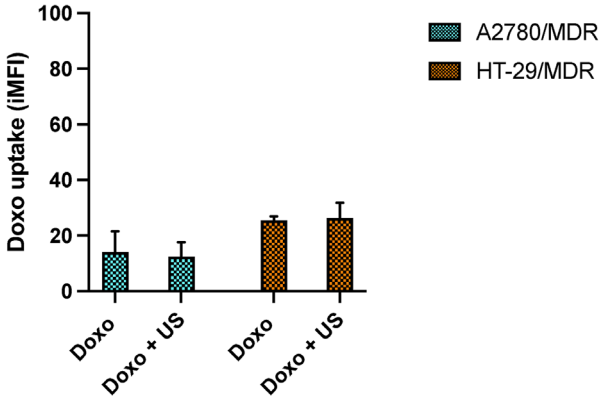

Figure 6. Doxo cellular uptake in MDR cell lines before and just after US exposure. A2780/MDR and HT-29/MDR cells were exposed to Doxo 0.5 and 1.0 μM for 1 h, respectively, and subsequently exposed to US (0.63 W cm^{-2}, 1.505 MHz, 3 min, 70% DC). Results are expressed as integrated mean of fluorescence intensity (iMFI).

compared to untreated cells ($p \leq 0.001$) (**Figure 8**). These data confirm the ability of US exposure to elicit cytotoxicity in both resistant cell lines thanks to the sonodynamic activation of the drug entrapped into the cell membrane or nearby the cell membrane.

2.7. Effects on Mitochondrial Function of Sonodynamic Treatment on A2780/MDR and HT-29/MDR 2D Cell Cultures

Since mitochondria play a central role for a variety of cellular processes such as intracellular ROS generation and Ca^{2+} signaling,[21] the mitochondrial functionality as mitochondrial membrane potential (MMP) has been investigated in both resistant cell lines immediately after SDT. The sonodynamic treatment of A2780/MDR cells induced a slight increase in fluorescent monomeric forms and a subsequent reduction in the aggregates-monomers ratio resulting in a not significant impairment of mitochondrial membrane potential. Interestingly, any significant difference in mitochondrial membrane potential has also been observed on HT-29/MDR cells immediately after SDT, as the mitochondrial function was very similar to that of untreated cells (**Figure 9**).

2.8. Induction of ICD-Related DAMPs by Sonodynamic Treatment of A2780/MDR and HT-29/MDR 2D Cell Cultures

Calreticulin (CRT) is an important immunogenic cell death (ICD)-related damage-associated molecular pattern (DAMP) functioning mainly as an early "eat me signal" produced during the ICD.[22] As shown in **Figure 10**, CRT was investigated 6 h after each treatment resulting a significant increase only in SDT (Doxo + US treatment)-treated HT-29/MDR cells, compared to untreated cells ($p \leq 0.05$). Moreover, the occurrence of high mobility group box-1 (HMGB-1), a late ICD-related DAMP released from the nucleus in the late stage of ICD,[23] was also investigated 48 h after each treatment. No statistically significant increase in HMGB-1 was observed in the MDR cell lines compared to untreated cells.

2.9. Doxorubicin Cellular Uptake in HT-29/WT and HT-29/MDR Spheroids

As reported in Material and Methods, it was not possible to obtain stable 3D structure with A278/MDR cells so the proposed

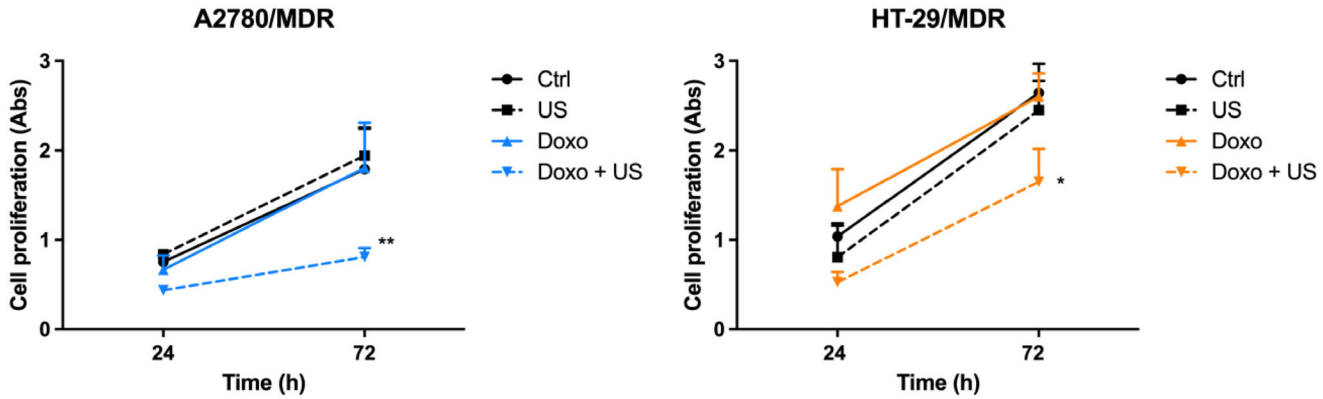

Figure 5. Effect on cell proliferation of the US exposure of Doxo-pre-incubated A2780/MDR and HT-29/MDR cells. A2780/MDR and HT-29/MDR cells were incubated for 1 h with Doxo 0.5 and 1.0 μM, respectively, and subsequently exposed to US (0.63 W cm^{-2}, 1.505 MHz, 3 min, 70% DC). Cell proliferation was assessed by using WST-1 assay after 24 and 72 h. Statistical significance versus untreated cells (Ctrl): $^{*}p \leq 0.05$, $^{**}p \leq 0.01$.

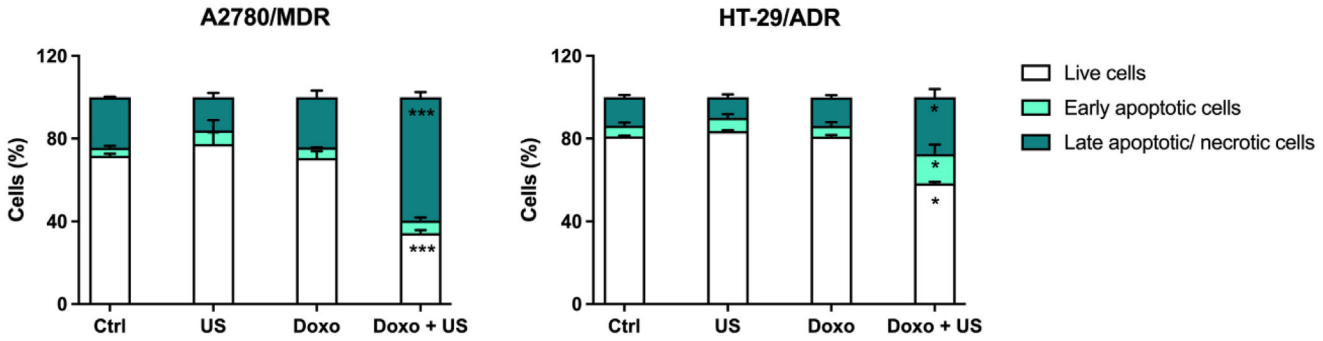

Figure 7. Cell death induced by US exposure of Doxo pre-incubated A2780/MDR and HT-29/MDR cells. A2780/MDR and HT-29/MDR cells were incubated for 1 h with Doxo 0.5 and 1.0 μM, respectively, and subsequently exposed to US (0.63 W cm^{-2}, 1.505 MHz, 3 min, 70% DC). Forty-eighth hours after the treatment, cells were incubated with Cell Death Apoptosis Kit and evaluated by flow cytometry. Statistical significance versus untreated cells (Ctrl): $^{*}p \leq 0.05$, $^{***}p \leq 0.001$).

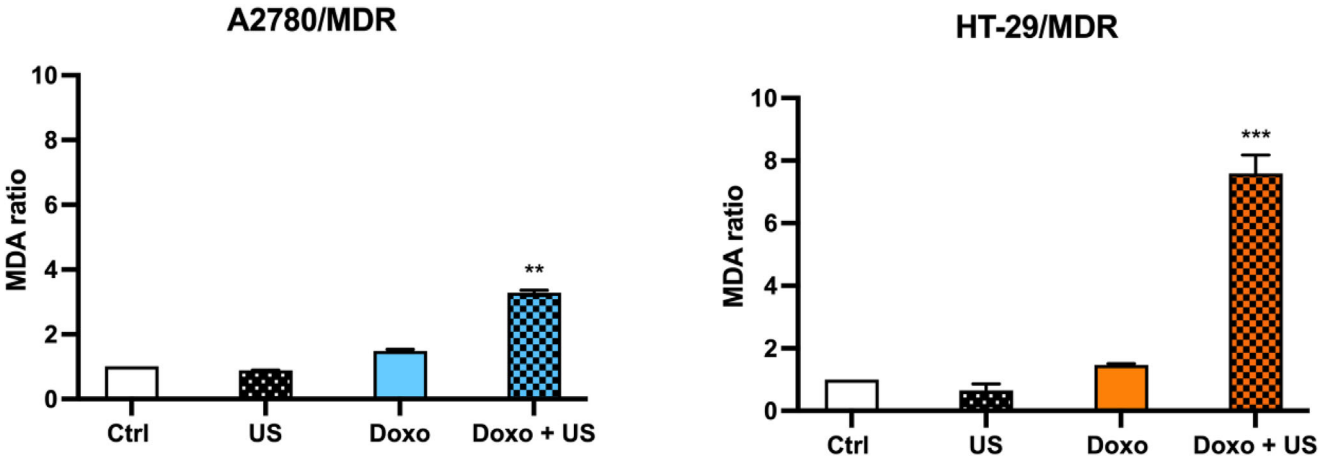

Figure 8. Lipid peroxidation induced by US exposure of Doxo pre-incubated A2780/MDR and HT-29/MDR cells. A2780/MDR and HT-29/MDR cells were incubated for 1 h with Doxo 0.5 and 1.0 μM respectively, and subsequently exposed to US (0.63 W cm^{-2}, 1.505 MHz, 3 min, 70% DC). After 36 h MDR cells were evaluated by flow cytometric analyses using the MDA Assay Kit. Data were expressed as MDA ratio between MDA nmol mL^{-1} of cells treated with Doxo and US and MDA nmol mL^{-1} of untreated cells (Ctrl). Statistical significance versus untreated cells (Ctrl): $^{**}p \leq 0.01$; $^{***}p \leq 0.001$.

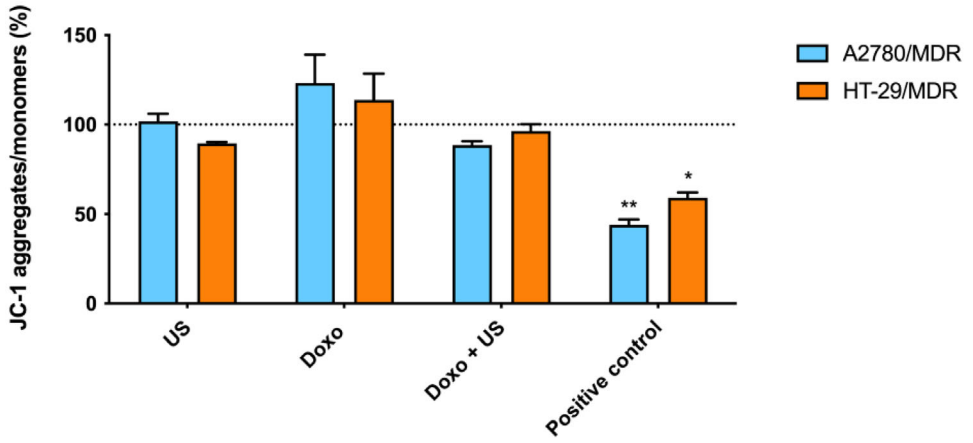

Figure 9. MMP after US exposure of Doxo pre-incubated A2780/MDR and HT-29/MDR cells. A2780 MDR and HT-29 MDR cells were incubated for 1 h with Doxo at 0.50 and 1 μM, respectively, and then exposed to US (0.63 W cm^{-2}, 1.505 MHz, 3 min, 70% DC). MMP was evaluated by JC-1 assay immediately after the treatments by flow cytometry and expressed as percentage of JC-1 aggregates to monomers fluorescence ratio in each sample. A positive control was obtained by exposing cells to H_2O_2 (500 μM) for 3 h. The mitochondrial membrane potential of untreated cells is represented by the dashed line. Statistically significant difference versus untreated cells: $^{*}p \leq 0.05$, $^{**}p \leq 0.01$.

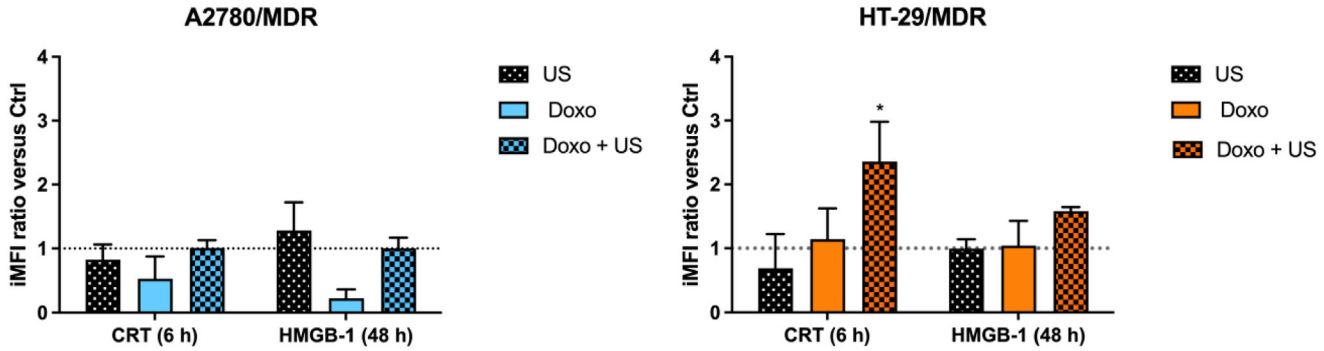

Figure 10. Evaluation ofCRT and HMGB-1 after SDT on A2780/MDR and HT-29/MDR cells. A2780/MDR and HT-29/MDR cells were incubated for 1 h with Doxo 0.5 and 1.0 μM, respectively, and subsequently exposed to US (0.63 W cm^{-2}, 1.505 MHz, 3 min, 70% DC). CRT and HMGB-1 occurrence were detected at 6 and 48 h after the treatment, respectively, and results were expressed as(iMFI ratio (CRT and HMGB-1 level in untreated cells is represented by the dashed line). Statistically significant difference of SDT-treated cells versus untreated cells: $^{*}p \leq 0.05$.

sonodynamic treatment was investigated only on HT-29/MDR spheroids. First, it was analyzed the Doxo uptake in HT-29/WT and HT-29/MDR spheroids by incubating the spheroids with increasing Doxo concentrations for 1 h to investigate the drug cellular internalization by flow cytometry. Observing **Figure 11**, HT-29/WT spheroids showed a dose-dependent increase in intracellular Doxo with statistically significance at 20 μM ($p \leq 0.05$), 30 μM ($p \leq 0.01$) and 100 μM ($p \leq 0.001$), compared to untreated spheroids (Ctrl); HT-29/MDR spheroids showed a statistically significant increase in intracellular Doxo only at 30 μM ($p \leq 0.05$) and 100 μM ($p \leq 0.05$), compared to Ctrl. These point out a different Doxo uptake between HT-29/WT and HT-29/MDR cells organized in 3D structure, as also observed in 2D cell cultures, due to the P-gp overexpression. Indeed, in HT-29/MDR spheroids the drug internalization was lower compared to HT-29/WT spheroids incubated with the same Doxo concentration. Therefore, for the subsequent sonodynamic experiments on HT-29/MDR spheroids, 20 μM was chosen as the appropriate Doxo concentration to be evaluated for sonodynamic treatment over 3D structures.

2.10. Effect of the US-Exposure of Doxo Pre-Incubated HT-29/MDR Spheroids

By considering the Doxo uptake in HT-29/MDR spheroids (Figure 11), HT-29/MDR spheroids were incubated with Doxo 20 μM for 1 h and then exposed to US. Spheroids were observed by optical microscopy measuring their volumes 24 and 48 h after the treatment. A slight reduction in spheroid volumes after SDT (Doxo + US treatment) was observed only after 48 h compared to untreated spheroids ($p \leq 0.05$) along with structural non-uniformity of the external crown compared to untreated spheroids (**Figure 12**), visible in the highlighted red quadrants.

Furthermore, to deeply investigate the cell death induced by the treatment, spheroids have been stained with propidium iodide (PI) to detect necrotic cells 48 h after the sonodynamic treatment and then observed at fluorescence microscopy. A statistically significant increase in PI fluorescence intensity was observed in the spheroids pre-incubated with Doxo and then exposed to US compared to untreated spheroids (**Figure 13**). Moreover, it was also investigated the occurrence of ICD-related

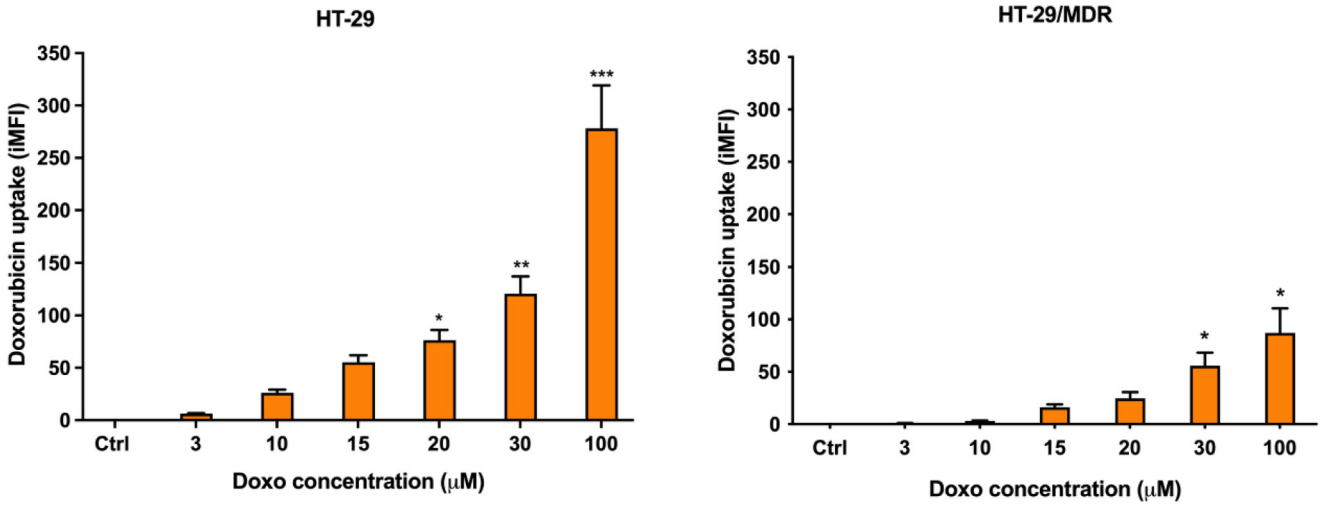

Figure 11. Doxo cellular uptake in HT-29/WT and HT-29/MDR spheroids. Spheroids were incubated with increasing Doxo concentrations (3, 10, 15, 20, 30, and 100 μM) for 1 h. Results were expressed as iMFI. Statistical significance versus untreated spheroids: $^{*}p \leq 0.05$, $^{**}p \leq 0.01$, $^{***}p \leq 0.001$.

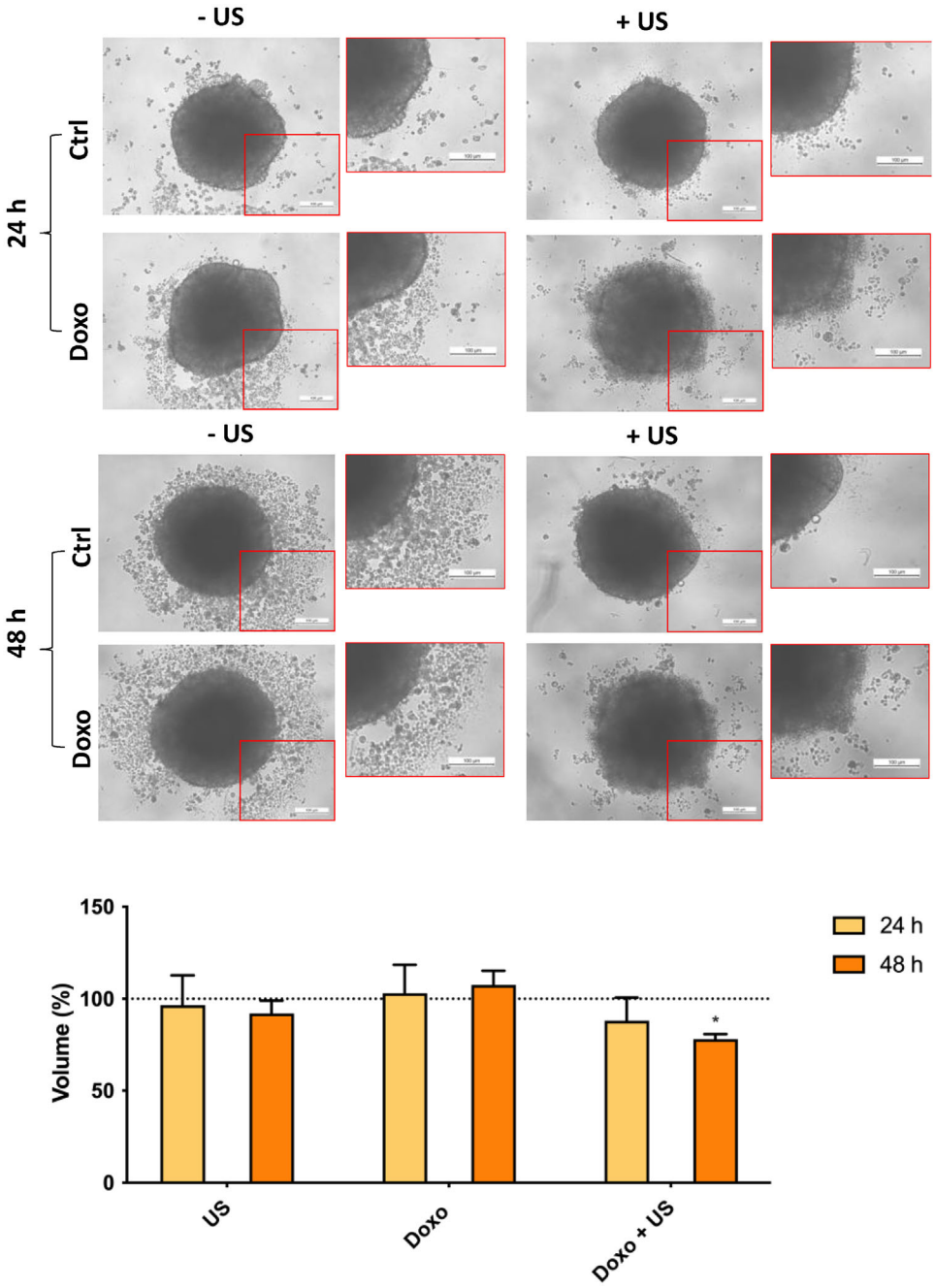

Figure 12. Effect of the US exposure of Doxo-pre-incubated HT-29/MDR spheroids. Spheroids were incubated with Doxo (20 μM) for 1 h and then exposed to US (1.66 W cm^{-2}, 1.505 MHz, 5 min, 70% DC). In the upper part of the figure, representative spheroids' images have been reported (magnification: 10x; scale bars: 100 μm) along with a 25% enlargement of the highlighted red quadrant. In the lower part of the figure, spheroids' volumes have been reported after 24 and 48 h from US exposure and results are expressed as volume percentage of treated spheroids versus untreated spheroids (the volume of untreated spheroids is represented by the dashed line). Statistical significance versus untreated spheroids (Ctrl): $^{*}p \leq 0.05$.

DAMPs in HT-29/MDR spheroids but no statistically significant results were obtained by considering CRT and HMGB-1 at the same time of occurrence in 2D cell cultures compared to untreated spheroids, although a slight increase in CRT and HMGB-1 expression has been observed (Figure 13).

3. Discussion

Drug resistance continues to be one of the main factors limiting the achievement of cure in cancer patients. Indeed, although many cancer types are initially sensitive to chemotherapy, over

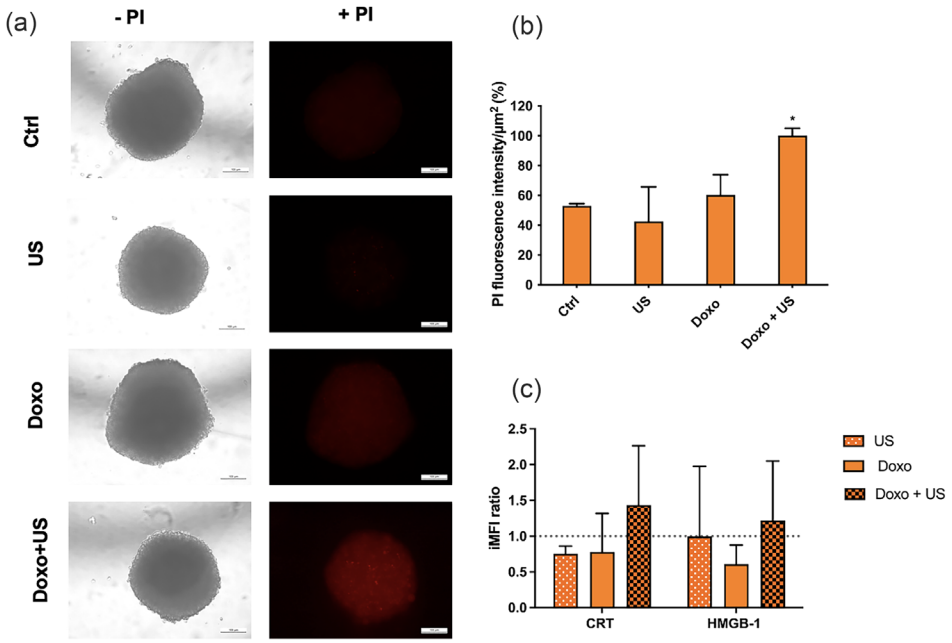

Figure 13. Evaluation of cell death and occurrence of CRT and HMGB-1 after SDT on HT-29/MDR spheroids. Spheroids were incubated with Doxo (20 μM) for 1 h and then exposed to US (1.66 W cm^{-2}, 1.505 MHz, 5 min, 70% DC). A) After 48 h, spheroids were stained with PI (100 μg mL^{-1}) (magnification: 10x; scale bars: 100 μm). B) PI fluorescence quantification as mean of percentage of PI intensity μm^{-2} ± SD. Statistically significant difference of treated spheroids versus untreated spheroids (Ctrl): $^{*}p \leq 0.05$. C) CRT and HMBG-1 occurrence was detected at 6 and 48 h after the treatment, respectively, and results were expressed asiMFI ratio (CRT and HMGB-1 level in untreated cells is represented by the dashed line).

time they can develop resistance through mechanisms such as: drug efflux, drug target alteration, drug inactivation, cell death inhibition, the epithelial-mesenchymal transition (EMT), DNA damage repair, epigenetic effects, or any combination of these mechanisms.[24]

Although new anti-cancer therapies have been introduced in recent decades, drug resistance still remains a challenge, so various strategies to overcome it are under investigation as the use of combination therapy, the use of P-gp inhibitors and/or substrates and the targeting of cancer stem cells.[25]

To investigate if our sonodynamic approach was able to overcome the P-gp mediated Doxo resistance, we have first identified the Doxo IC_{50} values at 24 h resulting ≈2 μM in HT-29/WT cells and higher than 100 μM in HT-29/MDR cells as was also observed in A2780/WT and A2780/MDR cells in an our previous work.[17] A very different cellular uptake of Doxo between the WT and the MDR cell lines was then highlighted by cytofluorimetric analysis (Figure 1). These data were consistent with studies showing that the overexpression of P-gp is responsible for the high efflux of Doxo from cancer cells,[26] and were confirmed by investigating in both cell lines the P-gp activity using the calcein-AM assay (Figure 2A) and the P-gp expression using an antibody-mediated detection (Figure 2B). Moreover, it was observed a peculiar Doxo cellular distribution as the drug was mainly localized at the membrane level in compact clusters on both MDR cell lines, probably due to P-gp activity (Figure 3).

Interestingly, US exposure of Doxo pre-incubated MDR cells was able to significantly inhibit cell proliferation in both A2780/MDR and HT-29/MDR cells at 72 h, whereas Doxo and US alone did not affect cancer cell proliferation (Figure 5). To the best of our knowledge, this demonstrates, for the first time, the synergistic cytotoxic effect of US and Doxo on HT-29/MDR, confirming the same effect already observed on A2780/MDR cells.[17]

To avoid any misinterpretation about the increased cytotoxicity of Doxo obtained with our US set up, a cytofluorimetric assay was performed to investigate a possible US-induced sonoporation mechanism in both resistant cell lines (Figure 6). As no increase in the Doxo uptake after US exposure was observed, it is possible to assume that the Doxo cytotoxicity was due to a sonodynamic activation of Doxo rather than to an increase in the drug uptake by sonoporation. This achievement was also consistent with the work by Fant and colleagues in which the morphological observation of cells by confocal microscopy did not show any membrane poration differences in US-exposed and non-US-exposed cells.[27]

Given that our sonodynamic approach killed the MDR cell lines, we decided to investigate the SDT-induced cell death at 48 h after SDT. A significant reduction in live cells was then observed in both A2780/MDR and HT-29/MDR cells along with a significant increase in late apoptotic/necrotic cells even if at a different extent in the two resistant cell lines (Figure 7).

Since in our previous work[17] we showed that the underlying mechanism of action triggering the cytotoxic effects of Doxo on A2780/MDR cells was based on intramembrane ROS-production, an evaluation of the lipid peroxidation was performed evaluating the most used lipid marker of oxidative stress, namely malondialdehyde (MDA). Interestingly, a strong level of lipid peroxidation was observed in HT-29/MDR cells after SDT compared to untreated cells (Figure 8). Therefore, according to the localization of Doxo in resistant cells (Figure 3) and the hypothesis of the BLS suggested by Krasovitski et al.,[19] it

is possible to assume that the US-induced ROS generation in SDT predominantly targeted the plasma membrane. This suggestion could be also confirmed by the results from cell-death analyses that showed mainly a necrotic cell death due to lipid peroxidation.

To complete our study on the role of the oxidative stress in the cytotoxicity induced by SDT with Doxo in MDR cell lines, an investigation of mitochondrial membrane potential was performed because it has been reported that ROS can act directly on mitochondria, provoking their dysfunction and leading to a progressive decrease in mitochondrial-membrane potential.[28,29] Interestingly, no impairment of the mitochondrial function was observed in both resistant cell lines, confirming the plasma membrane as the main ROS target in the sonodynamic treatment of MDR cells (Figure 9).

Considering these results and the fact that the effects of SDT on HT-29/MDR cells are very similar to those on A2780/MDR cells, it can be assumed that the sonodynamic approach was able to overcome the P-gp mediated resistance to Doxo in the two different cell lines through the same underlying mechanism.

To further confirm these achievements, the membrane fluidity of the MDR cell lines was investigated before and after US exposure, since we have already showed that different plasma membrane fluidity according to BLS theory can affect the selectivity and effectiveness of SDT on cancer cells.[30] Indeed, in our previous work it was shown that in the HT-29/WT cell line a change in membrane fluidity after US exposure could be related to the responsiveness to SDT, behavior confirmed also in this work in A2780/MDR and HT-29/MDR cells (Figure 4). Therefore, this could suggest that the cytotoxicity of SDT in A2780/MDR and HT-29/MDR cells might be primarily based on the mechanical properties of the plasma membrane, in accordance with the BLS theory. This means that the sonodynamic anticancer approach could not be affected by the occurrence of P-gp mediated resistance, since US exposure appears to be able of triggering the cytotoxicity of Doxo even at very low concentrations due to P-gp activity. Moreover, it was also explored the SDT ability to act as an ICD inducer, with CRT cellular exposure and HMGB-1 nuclear release. In our previous work on A2780/WT a significant increase in CRT cellular exposure, HMGB-1 nuclear release and ATP release after SDT was observed, suggesting that the activation of Doxo through US was able to kill A2780/WT cells in a way that might activate the ICD pathway.[31] Unfortunately, we did not see the same pattern in both A2780/MDR and HT-29/MDR cells (Figure 10). This point deserves further investigation even if we can hypothesize that this difference in ICD induction can be related to the main target of the SDT-induced oxidative stress being the cell membrane in MDR cells and the mitochondria in WT cells.

Finally, we moved from 2D MDR cell cultures to 3D MDR cell cultures since 3D models are an alternative strategy to represent reliable cell interactions and organization for preclinical investigation of new anticancer therapeutic approaches.[32] 3D models seem to be more representative than 2D models of the cells-matrix interactions, cellular migration in space and chemotherapeutic drug resistance.[32] Among several 3D models, the agarose coating technique represents a valid method for generating spheroids with high reproducibility, cost-effectiveness, and easy monitoring.[33,34]

According to the different structural organization of the spheroids, was therefore necessary to first evaluate the Doxo uptake into 3D spheroids compared to 2D cell monolayers. The proper Doxo concentration for SDT studies has been evaluated according to the quantification of intracellular Doxo by flow cytometry, focusing also on its effect on spheroid morphology and dimension by imaging analyses. Interesting is to highlight the difference in Doxo internalization between HT-29/WT and HT-29/MDR spheroids mirroring the one observed in 2D cell cultures, due to the different P-gp expression in the two cells lines. Preliminary results obtained by modifying the US parameters with respect to those used on 2D cell cultures, confirm the ability of SDT with Doxo to decrease the growth of Doxo-resistant spheroids by inducing a significant necrotic cell death even if to a lesser extent compared to what observed on 2D cell cultures. Noteworthy, the occurrence of ICD-related DAMPs was not observed after SDT on HT-29/MDR spheroids by considering the same time of observation of 2D cell cultures. As in 3D models, many factors can influence each other as cell adhesion and stiffness,[35,36] impacting on treatment response, a better tuning of US parameters is needed, possibly guided by the analysis of the US-effect on cell membrane fluidity into 3D structures.

4. Conclusion

Resistance to chemotherapy, especially to Doxo, represents one of the main challenges in cancer treatment. In this work we propose a new therapeutic strategy based on US, the so-called sonodynamic therapy, establishing its efficacy in different Doxo-resistant cell lines and suggesting the underlying mechanism able to overcome the P-gp-mediated resistance to Doxo. In fact, this approach, being characterized by the use of very low concentrations of Doxo that are not cytotoxic per se, but cytotoxic only after US exposure, exploits the US ability of influencing the cell membrane fluidity where, according to the BLS theory, the cytotoxic activity of Doxo is triggered even in drug-resistant cells. Finally, the study also conducted on 3D models seems to confirm the efficacy of this approach, although further studies will certainly be needed.

5. Experimental Section

A2780 and HT-29 2D and 3D Cell Cultures: The human ovarian cancer cell line A2780/WT and its counterpart resistant to Doxo, A2780/MDR, were purchased from the European collection of authenticated cell cultures (ECACC, Salisbury, UK). A2780/WT cells were obtained from an ovarian endometroid adenocarcinoma of an untreated patient while the resistant phenotype was acquired by exposing the cells to Doxo. The human adenocarcinoma colon cancer cell line, HT-29/WT was obtained from the American Type Culture Collection (ATCC, LGC, Milano, Italy) while its counterpart resistant to Doxo, HT-29/MDR, was kindly provided by Prof. Chiara Riganti (Department of Oncology, University of Torino, Italy).

A2780/WT and HT-29/WT cell lines were cultured as monolayers in cell culture flasks (Techno Plastic Products, TPP, Trasadingen Switzerland) and maintained in growth medium RPMI-1640 (Merck, Milano, Italy), supplemented with 10% of foetal bovine serum (FBS, Lonza, Verviers, Belgium), 2 mM L-glutamine, streptomicin (100 µL mL^{-1}) and penicillin (100 µg mL^{-1}) (Merck). A278/MDR and HT-29/MDR cell lines were cultured as monolayers in complete growth medium supplemented with Doxo (0.1 µM, Merck), in order to preserve the drug resistance. All cell lines

were cultured in a humidified ambient, protected from light, at 37 °C and 5% of CO_2, in an incubator (Thermo Fisher Scientific, Waltham, MA, USA), and detached, at 75% of confluence, by using 0.05% trypsin-0.02% EDTA (Merck).

HT-29/WT and HT-29/MDR spheroids were obtained adopting the agarose coating technique. Agarose (Merck) was stored at 4 °C, repaired from light and resuspended in phosphate buffer saline (PBS, Merck) before the use at the final concentration of 1.5%. The solution underwent to an autoclave sterilization cycle. At the end of the process, agarose was maintained in a hot bath water to avoid its solidification while 60 µL of solution were added into each well of a 96-U well plate (BRAND GMBH + CO KG, Wertheim, Germany). The plates were then left to cool down for 15 min and stored 24 h in a dark room. Cells were then detached at their 80% of confluence and seeded at the density of 5.0×10^3 cells/200 µL medium. Spheroid's growth and conformation were monitored by using Leica DMI4000B fluorescent microscope 10x (Leica Microsystems, Milano, Italy). Noteworthy, for A2780/WT and A2780/MDR cell lines it was not possible to realize spheroids by using the agarose coating technique, because spheroids obtained did not present a stable conformation. Therefore, only the HT-29/WT and HT-29/MDR spheroids were used as 3D in vitro cancer model.

Doxorubicin Cytotoxicity Assay in A2780 and HT-29 Cell Lines: Doxorubicin hydrochloride (Doxo, molecular weight 543.52 g mol^{-1}) was purchased as red lyophilized powder (Merck) resuspended in dimethyl sulfoxide (DMSO) at a concentration of 12 mM and then aliquoted to small volumes (100 µL) for storage at −20 °C, protected from light. Doxo 12 mM was diluted in RMPI-1640 medium (Sigma–Aldrich) to obtain the proper concentrations for experimental medium. The Doxo IC_{50} (the drug concentration needed to inhibit 50% of cell growth) in A2780/WT and A2780/MDR cells were obtained in a previous work.[17]

In order to evaluate the Doxo cytotoxicity and calculate its IC_{50} in HT-29/WT and HT-29/MDR cell lines, 1.5×10^3 cells were seeded in 96-well plates (TPP) in 100 µL of culture medium in replicates (n = 6) and then incubated with increasing concentrations of Doxo (0.00001, 0.0001, 0.001, 0.01, 0.1, 1, 10, and 100 µM). WST-1 assay (Roche Applied, Basel, Switzerland) was used to assess cell proliferation with the WST-1 reagent (10 µL) being added after 24 h and incubated for 3 h at 37 °C. The absorbance (abs) of the well was determined at 450 nm and 620 nm was used as reference wavelength in a microplate reader (Asys UV340; Biochrom, UK). Cytotoxicity was displayed as a percentage in agreement with the equation: % cytotoxicity = $100 \times (abs_{control} - abs_{sample})$. Doxo IC_{50} was then calculated using CalcuSyn software (Biosoft, Cambridge, UK, version 2.0). Moreover, the IC_{05}, i.e., the drug concentration needed to inhibit 0.5% of cell, was also calculated to select the proper non-cytotoxic concentration of Doxo to act as a sonosensitizer for the US-based treatment in all cell lines.

Fluorescence Microscopy: Fluorescence microscopy was performed using a DMI4000B fluorescence microscope with a LAS acquisition system (Leica, Wetzlar, Germany, version 3.8.0) and the acquired images were analyzed by ImageJ software (Fiji, Bristol, UK, version 2.0).

Doxorubicin Cellular Localization in A2780/MDR and HT-29/MDR Cell Lines: Fluorescence microscopy was used to investigate the localization of Doxo into the A2780/MDR and HT-29/MDR cells compared to A2780/WT and HT-29/WT cells. Briefly, 1×10^5 A2780/WT, A2780/MDR, HT-29/WT and HT-29/MDR cells were seeded on glass coverslips in 24-well plates; A2780/WT and A2780/MDR cells were then treated with Doxo 0.50 µM for 1 h and HT-29/WT and HT-29/MDR cells with Doxo 1.0 µM for 1 h. The slides were then washed with PBS and underwent to a fixation for 15 min with 4% paraformaldehyde (Merck). An incubation with DAPI for 15 min was used to stain cell nuclei. Finally, fluorescence images were collected at 40x magnification with an oil-immersion objective.

Cell Death Evaluation on HT-29/MDR 3D Cell Cultures: Forty-eight hours after Doxo + US treatment, cell damage on the corona of HT-29/MDR spheroids was investigated by staining spheroids with PI (Merck). Briefly, spheroids were washed twice with PBS to eliminate excess of experimental medium, and then incubated with a solution of PI in PBS (100 µg mL^{-1}) for 20 min in the dark at RT. When the incubation ended, PBS was used again twice to wash spheroids to remove PI excess and PI fluorescence images were then acquired (λ_{ex} 540 nm and λ_{em} 590 nm) and analyzed to quantify the PI fluorescence of HT-29/MDR spheroids, expressing the results as mean value of PI intensity/μm^2 ± standard deviation (SD).

SDT with Doxorubicin on A2780/MDR and HT-29/MDR 2D and 3D Cell Cultures: A2780/MDR and HT-29/MDR cells as 2D cell cultures were incubated respectively with Doxo 0.50 and 1 µM for 1 h, respectively. Cells were then detached and for each condition 5×10^5 cells were resuspended in a polystyrene tube (TPP) in 2.7 mL of PBS (Merck) that was opportunely connected to the US transducer by a mechanical adaptor filled with ultrapure cold water. The US field was generated with a piezoelectric transducer, responsible for US propagation, working in pulsed mode (DC) at 1.505 MHz, connected to a function generator (Type 33 250; Agilent, Santa Clara, CA, USA) and a power amplifier (Type AR 100A250A; Amplifier Research, USA).

The US treatment of both cell lines was performed at a power of 0.63 W cm^{-2} and a frequency of 1.505 MHz for 3 min at 70% DC. After US exposure, 1.2×10^3 cells/100 µL medium were seeded in 96-well plates in replicates for each condition (n = 6) and cell proliferation was evaluated with WST-1 assay (Roche Applied) by incubating the plates for 3 h in controlled conditions (37 °C, 5% CO_2) after 24 and 72 h from US exposure, as previously described. Data were expressed as mean value of abs ± SD.

The same US set-up was used for the treatment of HT-29/MDR cells as 3D cell cultures but with a modified power intensity and US time exposure. Briefly, 4 days after seeding, a total of 10 HT-29/MDR spheroids were selected per condition and placed in 2.7 mL PBS in polystyrene tubes to undergo the following treatments: control (i.e., untreated), US (1.66 W cm^{-2}, 1.505 MHz, 5 min, 70% DC), Doxo (20 µM for 1 h), and Doxo (20 µM pre-incubated for 1 h) + US (1.66 W cm^{-2}, 1.505 MHz, 5 min, a 70% DC). Treatment efficacy was then evaluated after 48 h by fluorescence microscopy and flow cytometric analyses.

Flow Cytometry: Flow cytometric analyses were assessed by using a C6 flow cytometer (Accuri, Milano, Italy) considering 10 000 events at medium flow rate, excluding the cellular debris with low side scatter (SSC) and forward scatter (FSC) from the evaluations; cytofluorimetric evaluations were performed using FCS Express software, version 4 (BD, Biosciences, Milano, Italy).

Cellular Uptake of Doxorubicin in A2780 and HT-29 2D and 3D Cell Cultures: For each cell lines cultured as 2D cell cultures, 8.0×10^4 cells/1.5 mL medium per well were seeded in 6-well plates and incubated with two different non-cytotoxic concentrations of Doxo (0.05 and 0.50 µM in A2780/MDR cells and 0.5 and 1.0 µM in HT-29/MDR cells) after 1, 6, 12, and 24 h of incubation. At the end of Doxo incubation, cells were detached and resuspended in 200 µL of PBS and then evaluated by flow cytometry thanks to the intrinsic fluorescence of the drug (λ_{ex} 488 nm, λ_{em} > 670 nm). Data were expressed as iMFI obtained by the product between the frequency of Doxo positive cells and the mean fluorescence intensity of the cells. Moreover, to exclude a possible involvement of US in influencing Doxo uptake in resistant A2780 and HT-29 cells through a sonoporation mechanism, a cytofluorimetric investigation of intracellular Doxo has also been performed just after US exposure. Briefly, A2780/MDR and HT-29/MDR pre-incubated for 1 h with Doxo (0.5 and 1.0 µM, respectively) were exposed to US treatment (0.63 W cm^{-2}, 1.505 MHz, 5 min, 70% DC) and analyzed by flow cytometry immediately after the treatment.

For HT-29/MDR cell lines cultured as 3D cultures, 4 days after the seeding, HT-29 MDR spheroids were incubated with Doxo for 1 h at different Doxo concentrations (3, 10, 15, 20, 30, and 100 µM). After Doxo incubation, four spheroids for each condition were put into a sterile eppendorf tube and incubated for 15 min with 0.05% trypsin-0.025% EDTA at 37 °C. After trypsin inactivation and centrifugation, cells dissociated from 3D structures were washed in PBS and Doxo uptake determined by flow cytometry (λ_{ex} 488 nm, λ_{em} > 670 nm) and expressed as iMFI.

Calcein-AM Assay in A2780/MDR and HT-29/MDR Cell Lines: Calcein-AM (Merck) uptake was evaluated in each cell line to confirm the presence of a resistant phenotype. Indeed, calcein-AM is recognised as P-gp substrate.[37] 1.0×10^5 cells were incubated with 2 µL of calcein-AM in 1 mL of PBS and then incubated at 37 °C for 15 min. Cytofluorimetric eval-

uation was assessed flow cytometry (λ_{ex} 490 nm, λ_{em} 515 nm). Data were expressed as iMFI values ± SD.

Evaluation of P-gp Expression in A2780 and HT-29 Cell Lines: P-gp expression was evaluated in each cell line using the mouse anti P-gp primary antibody (cat. n. ab3366, Abcam, Cambridge, UK, 1:200) by considering 2.0×10^5 cells and 30 min of reaction at room temperature (RT). At the end of incubation, cells were washed with PBS, centrifugated and incubated with the goat anti-mouse secondary antibody conjugated with Alexa Fluor 647 (cat. n. 150 119, Abcam) for 1 h at RT. After the incubation, cells were washed with PBS, centrifuged and then analyzed by flow cytometry (λ_{ex} 650 nm, λ_{em} 665 nm). Results were presented as distribution plot presenting the number of staining-positive cells in function of the fluorescence intensity.

Evaluation of Membrane Fluidity on A2780 and HT-29 Cell Lines: Membrane fluidity was evaluated by using MC540 (Merck), a lipophilic fluorescent dye reacting with the outer leaflet of the cellular membranes. MC540 fluorescence intensity is influenced by changes in membrane fluidity; MC540 increases its affinity as the membrane lipid components become more disordered.[38] A2780 and HT-29 cells, and their resistant counterparts were detached, and 2.0×10^5 cells were incubated with 25 nM of MC540 for 15 min at room temperature, protected from light. At the end of incubation, flow cytometric analysis (λ_{ex} 555 nm, λ_{em} 578 nm) was assessed. Results were expressed as iMFI of MC540 positive cells. Moreover, to evaluate if membrane fluidity can be influenced by US, a cytofluorimetric evaluation of membrane fluidity was also performed immediately after US exposure. Briefly, A2780/MDR and HT-29/MDR cells underwent to US treatment (0.63 W cm^{-2}, 1.505 MHz, 3 min, 70% DC) and at the end of treatment, samples were centrifuged to eliminate PBS and the cells pellet incubated with 25 nM of MC540 for 15 min at room temperature, protected from light. Flow cytometric analysis was then assessed and resulted expressed as previously described.

Cell Death Evaluation on A2780/MDR and HT-29/MDR 2D Cell Cultures: Cell death was evaluated using the Cell Death Apoptosis Kit (Life Technology, Milan, Italy) 48 h after SDT (Doxo + US treatment). The kit contains APC-annexin V, which can bind phosphatidylserine expressed on the surface of apoptotic cells, and Sytox Green that instead reacts with nuclei and enters in both late apoptotic and early apoptotic cells; late apoptotic/necrotic cells are positive for both Sytox Green and APC-annexin V staining, apoptotic cells are negative for Sytox Green and positive for APC-annexin V staining, whereas viable cells are negative for both staining. After SDT, A2780/MDR and HT-29/MDR cells were seeded in 6-well plates (5×10^5/1.5 mL medium for each well), detached 48 h after with 0.05% trypsin-0.025% EDTA, stained with APC-annexin V and Sytox Green and then evaluated by flow cytometry (λ_{ex} 640 nm and λ_{em} 675/25 nm for APC-annexin V; λ_{ex} 488 nm and λ_{em} 533/30 nm for Sytox Green). Results were expressed as percentage of live, late apoptotic/necrotic and early apoptotic cells for each condition of treatment.

Lipid Peroxidation Assay in A2780/MDR and HT-29/MDR 2D Cell Cultures: The evaluation of the lipid peroxidation induced by SDT (Doxo + US treatment) was performed using the Lipid Peroxidation (MDA) Assay Kit (cat. n. ab118970, Abcam). Following manufacturer's instructions, MDA was evaluated in cells under the different treatments (US, Doxo or Doxo + US) after 36 h in A2780/MDR and HT-29/MDR cells. MDA is one of the products of lipid peroxidation chain and its detection reveals the presence of damage induced by this type of stress, representing an important marker for highlighting oxidative stress and moreover, it could be estimated this effect by MDA quantification.[39] MDA binds thiobarbituric acid (TBA) determining the generation of MDA-TBA adducts, which then is detected thanks to the colorimetric properties. [39] After the Doxo + US treatment, MDA assay was performed according to manufacturer's instruction and the 96-well plates were analyzed by using a microplate reader (Asys UV340; Biochrom), at the wavelength of 540 nm. Results were expressed as MDA ratio between the nmol mL^{-1} of MDA in treated cells and nmol mL^{-1} of MDA in untreated cells (Ctrl).

Mitochondrial Membrane Potential Assay in A2780/MDR and HT-29/MDR 2D Cell Cultures

The effects that sonodynamic treatment had on the mitochondrial function of A2780/MDR and HT-29/MDR cells have been investigated using the Membrane Potential Detection Kit (BD Bioscience, San Jose, CA, USA). This assay relies on JC-1, a double fluorescent dye used to monitor the MMP, that can be observed as green fluorescent monomers or red fluorescent aggregates. JC-1 does not accumulate in mitochondria with depolarized MMP remaining in the cytoplasm as monomers.

Briefly, A2780/MDR and HT-29/MDR cells were incubated for 1 h with Doxo 0.5 and 1 µM, respectively, at 37 °C and then exposed to US, as previously described. Moreover, a positive control was performed by exposing both cell lines to 500 µM H_2O_2 for 3 h. Immediately after each treatment, JC-1 aggregates and monomers were investigated for each condition by flow cytometry (λ_{em} 532 nm and λ_{em} 585 nm). Regions were placed around the cell populations with high JC-1 aggregates and monomers concentration (functional mitochondria), other regions were placed around cell populations with low JC-1 aggregates and high JC-1 monomers concentration (less functional mitochondria). For quantitative analysis, mitochondrial membrane potentials were expressed as the ratio between JC-1 aggregate and monomer mean fluorescence emission.

Evaluation of Immunogenic Cell Death-Related Damage Associated Molecular Patterns in A2780/MDR and HT-29/MDR 2D Cell Cultures: CRT exposure on cell surface was investigated 6 h after SDT (Doxo + US treatment) of A2780/MDR and HT-29/MDR 2D cell cultures. Briefly, cells were washed with PBS, incubated with 0.05% trypsin-0.025% EDTA for 5 min at 37 °C and followed by incubation with 10 µg mL^{-1} of Alexa Fluor 488 anti-CRT antibody (cat. n. ab196158, Abcam) at RT for 40 min, in dark condition. After the incubation, cells were washed twice with PBS and then analyzed by C6 flow cytometer (λ_{ex} 488 nm, λ_{em} 530 nm).

HMGB-1 occurrence was determined 48 h after the Doxo + US treatment of A2780/MDR and HT-29/MDR 2D cell cultures. Briefly, cells were washed with PBS, incubated with 0.05% trypsin-0.025% EDTA for 5 min at 37 °C and then with anti-HMGB-1 antibody (10 µg mL^{-1}; cat. n. ab77302, Abcam) for 30 min at RT, in dark condition. When the incubation ended, cells were washed once with PBS and then incubated with anti-mouse immunoglobulin G (whole molecule)-fluorescein isothiocyanate (FITC) antibody (1:200; cat n. SAB4200738, Sigma-Aldrich) for 1 h at RT, in dark condition. Finally, cells were washed twice with PBS at the end of incubation and then analyzed by C6 flow cytometer (λ_{ex} 488 nm, λ_{em} 530 nm).

For HT-29/MDR 3D cultures, 6 and 48 h after the treatments 18 spheroids per condition have been considered, collected in a tube, processed with 0.05% trypsin-0.025% EDTA at 37 °C for 15 min to obtain single cell suspension and then incubated with anti-CRT and anti-HMGB1 antibodies, respectively, as detailed above for 2D cell cultures before proceeding with flow cytometry analysis.

Statistical Analysis: Data are the result of three independent experiments and are expressed as mean ± SD. Graph-Pad Prism 10.0 (La Jolla, CA, USA) was used for elaborating the data. To assess the statistical significance threshold ($p \leq 0.05$) multiple t-tests, two-way ANOVA, one-way ANOVA and Bonferroni's test were used based on the design of the experiment under analysis.

Acknowledgements

This research was funded by the Associazione Italiana per la Ricerca sul Cancro (AIRC, IG-22041), the Ministero dell'Università e della Ricerca (MUR) (Progetti di Ricerca di Rilevante Interesse Nazionale – PRIN 2022, 2022X,7ESJ3) and the University of Torino (Ricerca Locale 2023). The authors would also like to thank Prof. Giampiero Muccioli for his support and critical advice, and Sara Giordano for spheroid image-based analysis.

Open access publishing facilitated by Universita degli Studi di Torino, as part of the Wiley - CRUI-CARE agreement.

Conflict of Interest

The authors declare no conflict of interest.

Data Availability Statement

The data that support the findings of this study are available from the corresponding author upon reasonable request.

Keywords

cancer, doxorubicin, multidrug resistance, P-glycoprotein, sonodynamic therapy

Received: February 16, 2024
Revised: June 11, 2024
Published online: August 3, 2024

[1] N. Vasan, J. Baselga, D. M. Hyman, *Nature* **2019**, *575*, 299.
[2] X. Wang, H. Zhang, X. Chen, *Cancer Drug Resist.* **2019**, *2*, 141.
[3] C. Pilotto Heming, W. Muriithi, L. Wanjiku Macharia, P. Niemeyer Filho, V. Moura-Neto, V. Aran, *Heliyon* **2022**, *8*, e11171.
[4] T. Bin Emran, A. Shahriar, A. Rafi Mahmud, T. Rahman, M. Hasan Abir, M. faijanur-Rob Siddiquee, H. Ahmed, N. Rahman, F. Nainu, E. Wahyudin, S. Mitra, K. Dhama, M. M. Habiballah, S. Haque, A. Islam, M. Mahmudul Hassan, *Front. Oncol.* **2022**, *12*, 891652.
[5] R. Callaghan, F. Luk, M. Bebawy, *Drug Metab. Dispos.* **2014**, *42*, 623.
[6] M. Susa, A. K. Iyer, K. Ryu, E. Choy, F. J. Hornicek, H. Mankin, L. Milane, M. Amiji, Z. Duan, *PLoS One* **2010**, *5*, e10764.
[7] L. Milane, Z. Duan, M. Amiji, *PLoS One* **2011**, *6*, e24075.
[8] J. Gong, R. Jaiswal, J.-M. Mathys, V. Combes, G. E. R. Grau, M. Bebawy, *Cancer Treat. Rev.* **2012**, *38*, 226.
[9] Y. Yao, Y. Zhou, L. Liu, Y. Xu, Q. Chen, Y. Wang, S. Wu, Y. Deng, J. Zhang, A. Shao, *Front. Mol. Biosci.* **2020**, *7*, 193.
[10] F. Mottaghitalab, M. Farokhi, Y. Fatahi, F. Atyabi, R. Dinarvand, *J. Control Release* **2019**, *295*, 250.
[11] M. Majidinia, M. Mirza-Aghazadeh-Attari, M. Rahimi, A. Mihanfar, A. Karimian, A. Safa, B. Yousefi, *IUBMB Life* **2020**, *72*, 855.
[12] M. Paškevičiūtė, V. Petrikaitė, *Drug Deliv. Transl. Res.* **2019**, *9*, 379.
[13] R. Canaparo, F. Foglietta, N. Barbero, L. Serpe, *Adv Drug Deliv. Rev.* **2022**, *189*, 114495.
[14] T. Yamaguchi, S. Kitahara, K. Kusuda, J. Okamoto, Y. Horise, K. Masamune, Y. Muragaki, *Cancers* **2021**, *13*, 6184.
[15] Z. Gong, Z. Dai, *Adv. Sci.* **2021**, *8*, 2002178.
[16] V. Choi, M. A. Rajora, G. Zheng, *Bioconjug. Chem.* **2020**, *31*, 967.
[17] F. Foglietta, M. Macrì, P. Panzanelli, A. Francovich, G. Durando, F. Garello, E. Terreno, L. Serpe, R. Canaparo, *Eur. J. Pharm. Biopharm.* **2023**, *183*, 119.
[18] K. C. Nitiss, J. L. Nitiss, *Clin. Cancer Res.* **2014**, *20*, 4737.
[19] B. Krasovitski, V. Frenkel, S. Shoham, E. Kimmel, *Proc. Natl. Acad. Sci. USA* **2011**, *108*, 3258.
[20] A. Ayala, M. F. Muñoz, S. Argüelles, *Oxid. Med. Cell Longev* **2014**, *2014*, 1.
[21] A. V. Kuznetsov, R. Margreiter, M. J. Ausserlechner, J. Hagenbuchner, *Antioxidants* **2022**, *11*, 1995.
[22] Z. Asadzadeh, E. safarzadeh, S. Safaei, A. Baradaran, A. Mohammadi, K. Hajiasgharzadeh, A. Derakhshani, A. Argentiero, N. Silvestris, B. Baradaran, *Cancers* **2020**, *12*, 1047.
[23] S. T. Workenhe, J. Pol, G. Kroemer, *Oncoimmunology* **2021**, *10*, 1893466.
[24] G. Housman, S. Byler, S. heerboth, K. Lapinska, M. Longacre, N. Snyder, S. Sarkar, *Cancers* **2014**, *6*, 1769.
[25] A. Ramos, S. Sadeghi, H. Tabatabaeian, *Int. J. Mol. Sci.* **2021**, *22*, 9451.
[26] S. Mirzaei, M. Hossein Gholami, F. hashemi, A. Zabolian, M. Vasheghani Farahani, K. Hushmandi, A. Zarrabi, A. Goldman, M. Ashrafizadeh, G. Orive, *Drug Discov. Today* **2022**, *27*, 436.
[27] C. Fant, M. Lafond, B. Rogez, I. Suarez Castellanos, J. Ngo, J.-L. Mestas, F. Padilla, C. Lafon, *Sci. Rep.* **2019**, *9*, 15581.
[28] S. Gorini, A. De Angelis, L. Berrino, N. Malara, G. Rosano, E. Ferraro, *Oxid. Med. Cell Longev.* **2018**, *2018*, 1.
[29] F. Sivandzade, A. Bhalerao, L. Cucullo, *Bio Protoc.* **2019**, *9*, e3128.
[30] F. Foglietta, V. Pinnelli, F. Giuntini, N. Barbero, P. Panzanelli, G. Durando, E. terreno, L. Serpe, R. Canaparo, *Cancers* **2021**, *13*, 3852.
[31] D. Xie, Q. Wang, G. Wu, *Front. Immunol.* **2022**, *13*, 1017400.
[32] F. Foglietta, R. Canaparo, G. Muccioli, E. Terreno, L. Serpe, *Life Sci.* **2020**, *254*, 117784.
[33] C. Gong, Z. Kong, X. Wang, *Polymers* **2021**, *13*, 4028.
[34] X. Gong, C. Lin, J. Cheng, J. Su, H. Zhao, T. Liu, X. Wen, P. Zhao, *PLoS One* **2015**, *10*, e0130348.
[35] R. Demuynck, I. Efimova, F. Naessens, D. V. Krysko, *J. Immunother. Cancer* **2021**, *9*, e003430.
[36] K. M. Yamada, A. D. Doyle, J. Lu, *Trends Cell Biol.* **2022**, *32*, 883.
[37] Y.-T. Chang, Y.-C. Lin, L. Sun, W.-C. Liao, C. C. N. Wang, C.-Y. Chou, S. L. Morris-Natscke, K.-H. Lee, C.-C. Hung, *Phytomedicine* **2020**, *71*, 153239.
[38] J. Kaur, S. N. Sanyal, *Mol. Cell. Biochem.* **2010**, *341*, 99.
[39] D. Tsikas, *Anal. Biochem.* **2017**, *524*, 13.